ACS central science

http://pubs.acs.org/journal/acscii

Research Article

Light-Controlled Release of Therapeutic Proteins from Red Blood Cells

Brianna M. Vickerman, Colin P. O'Banion, Xianming Tan, and David. S. Lawrence*

Cite This: *ACS Cent. Sci.* 2021, 7, 93–103

Read Online

ACCESS | Metrics & More | Article Recommendations | Supporting Information

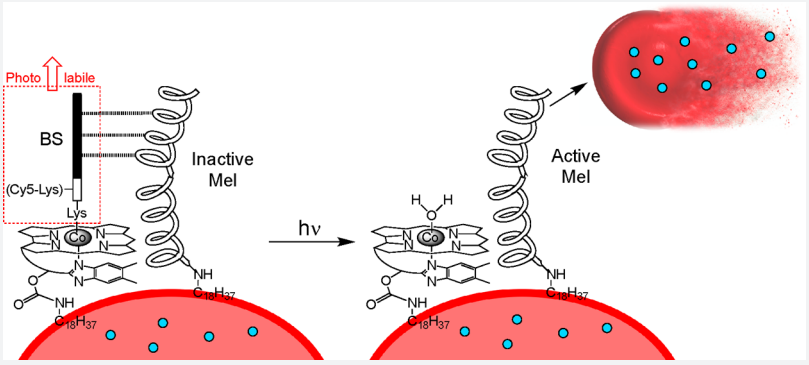

ABSTRACT: Protein therapeutics are a powerful class of drugs known for their selectivity and potency. However, the potential efficacy of these therapeutics is commonly offset by short circulatory half-lives and undesired action at otherwise healthy tissue. We describe herein a targeted protein delivery system that employs engineered red blood cells (RBCs) as carriers and light as the external trigger that promotes hemolysis and drug release. RBCs internally loaded with therapeutic proteins are readily surface modified with a dormant hemolytic peptide. The latter is activated via easily assigned wavelengths that extend into the optical window of tissue. We have demonstrated that photorelease transpires with spatiotemporal control and that the liberated proteins display the anticipated biological effects *in vitro*. Furthermore, we have confirmed targeted delivery of a clot-inducing enzyme in a mouse model. Finally, we anticipate that this strategy is not limited to RBC carriers but also should be applicable to nano- and microtransporters comprised of bilayer lipid membranes.

INTRODUCTION

Protein and peptide drugs have emerged as a dominant, rapidly growing class of therapeutic agents.[1,2] These drugs enjoy the advantages of potency and selectivity toward their biochemical target, particularly in comparison to traditional small molecule drugs.[1−4] In spite of these advantages, protein and peptide therapeutics, which are commonly given by infusion, often exhibit poor *in vivo* stability. These agents are highly susceptible to serum proteases and rapid renal clearance. As a consequence, peptide and protein drugs are typically dosed at high levels, resulting in narrow therapeutic windows.[1−5] This has resulted in clinical trial failures[6] as well as strict limitations on drugs that have received approval.[7]

There has been extensive research on protecting proteins from degradation by encapsulating protein therapeutics into drug carriers, including liposomes, nanoparticles, and red blood cells (RBCs).[2−5,8−13] RBCs are particularly noteworthy as carriers of therapeutic agents due to their long circulatory lifespan (∼4 months).[5,8,10−13] The two main strategies for appending drugs to RBCs include (1) internal encapsulation and (2) external conjugation to the membrane surface.[8,12,13] Although both approaches have distinct advantages and disadvantages, proteins embedded within the RBC interior enjoy the additional potential benefit of protection from serum proteases.[12] However, the challenge associated with RBC-conveyed transport is controlling the subsequent release of the therapeutic at the desired target site in a concentration sufficient to effect the desired salutary outcome.[2−4,8,13]

External stimuli, including ultrasound, heat, magnetism, and light, have been used to promote drug release from a host of engineered transporters, particularly nanocarriers.[14] The concept is straightforward: application of the stimulus limits drug/tissue interaction to only the diseased site, thereby protecting both the drug (from metabolic modification and excretion) and healthy tissue (from drug action).[4,14−16] Controlled release potentially offers enhanced drug delivery

Received: August 26, 2020
Published: December 9, 2020

https://dx.doi.org/10.1021/acscentsci.0c01151
ACS Cent. Sci. 2021, 7, 93−103

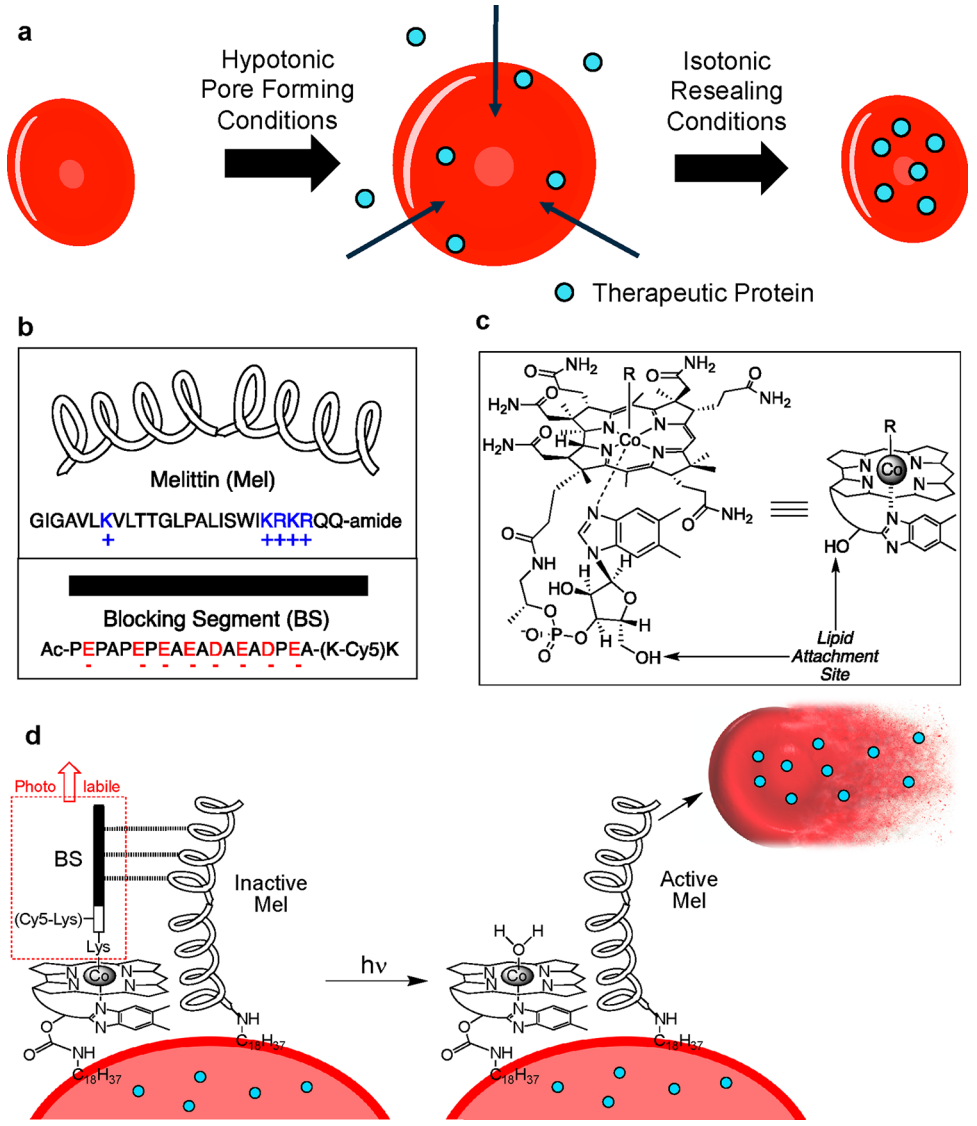

Figure 1. Assembly of a photohemolysis trigger on the surface of RBCs. **a.** Both human and mouse RBCs are first internally loaded with a therapeutic protein (blue circles) by sequential treatment with hypotonic conditions (pore formation), the protein of interest, and isotonic buffer (pore resealing). **b**. The photolytic trigger is composed of two peptides, melittin (Mel) and its pro-domain blocking segment (BS). **c.** Cobalamin (Cbl) is synthetically modified with a lipid, and the BS peptide is appended as a photocleavable ligand to Co. **d.** Simultaneous exposure of RBCs to the lipidated BS and Mel peptides generates a photoresponsive RBC construct (left). Upon illumination (525 nm for C_{18}-Cbl-BS or 660 nm for C_{18}-Cbl-Cy5BS), the BS peptide is released from Cbl, generating active Mel, subsequent hemolysis, and release of the internally loaded protein therapeutic. C_{18}-Cbl-Cy5BS (Scheme S4) is an analog of C_{18}-Cbl-BS that responds to 660 nm exposure.

to the diseased site, resulting in a larger therapeutic window and the consequent reduction in off-target toxicity.[4,14−18] We have re-engineered RBCs to convey and subsequently release internal protein cargo in response to preassigned wavelengths of light. Protein therapeutics are readily introduced into RBCs under hypotonic conditions, which generates pores in the erythrocyte plasma membrane. Restoration of isotonicity reseals the pores and entraps the protein drug (Figure 1a). To trigger the release of these protein therapeutics with light, our design strategy employs a photoactivatable, membrane-embedded, hemolytic peptide (Figure 1).

RESULTS AND DISCUSSION

Melittin (Mel), a 26-residue α-helical peptide, is a potent hemolytic agent that is a key component of European honey bee (*Apis mellifera*) venom (Figure 1b).[19] Mel has received extensive attention as a therapeutic agent due to its antimicrobial, anti-inflammatory, anticancer, and antidiabetic properties. However, these potentially useful biomedical applications are offset by the peptide's pronounced affinity for and lysis of RBCs.[19,20] We sought to take advantage of the latter property by transforming melittin into a light-triggered hemolytic agent.

Cobalamin (Cbl), also known as vitamin B12, is primarily available as one of four derivatives, each of which contains a different substituent (R) on the Co metal of the corrin ring (Figure 1c). The Co−C bond of methyl and adenosyl Cbl derivatives undergo homolytic cleavage upon illumination in the 330−550 nm range. We have previously taken advantage of this chemistry to photorelease a variety of small molecule drugs from the B12 scaffold (Cbl-Co-CH_2Drug).[21−24] Based on the known photosensitivity of the Co−C bond of alkyl-Cbls, we have prepared a quiescent, melittin-based, photohemolytic

https://dx.doi.org/10.1021/acscentsci.0c01151
ACS Cent. Sci. 2021, 7, 93−103

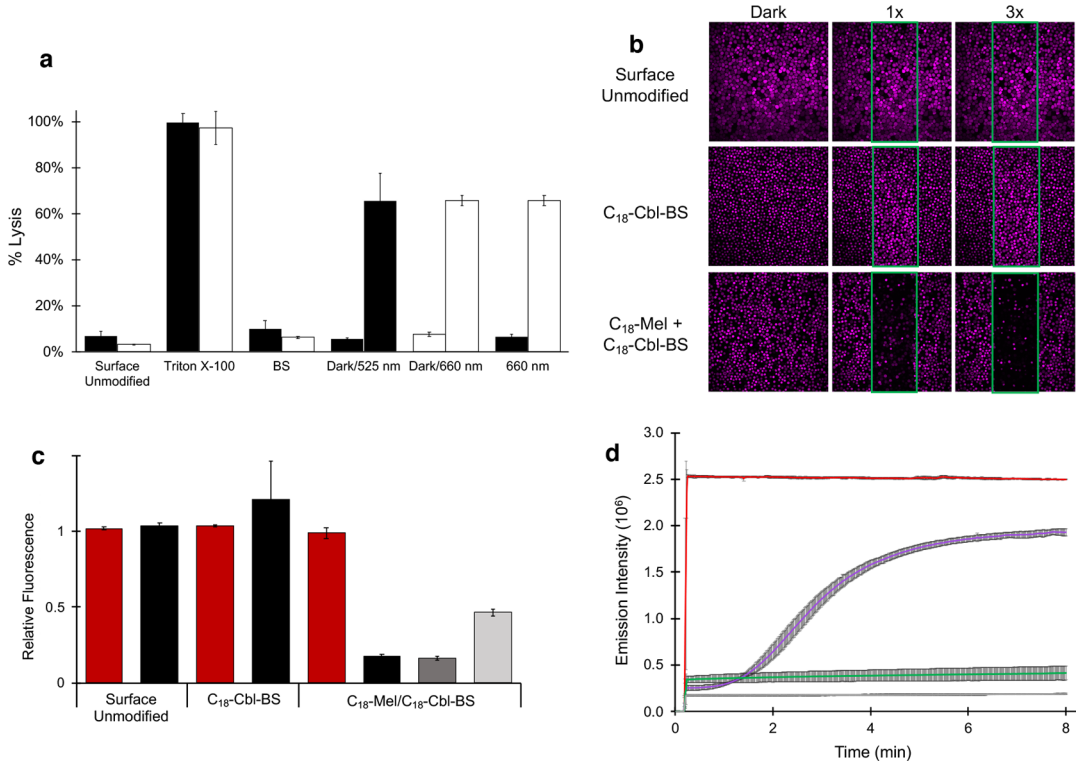

Figure 2. a. RBC lysis as a function of various conditions. BSA-TexasRed is embedded within the interior of RBCs. Following exposure of the RBCs to various conditions, the RBCs are centrifuged, and Texas Red fluorescence in the supernatant is taken as a measure of hemolysis. **Surface Unmodified** RBCs: Minimal lysis is observed with RBCs lacking a surface-anchored photolytic trigger that were illuminated with 525 nm (black bar) or 660 nm (white bar) LEDs. **Triton X-100**-treated RBCs with surface-anchored C_{18}-Cbl-BS/C_{18}-Mel (black bar) or C_{18}-Cbl-Cy5BS/C_{18}-Mel (white bar) are used as the 100% lysis control. **BS**-only surface-loaded RBCs exposed to 525 nm (black bar) or 660 nm (white bar) LEDs display minimal lysis due to the absence of C_{18}-Mel. **Dark/525 nm** (black bars) are RBCs containing surface-anchored C_{18}-Cbl-BS/C_{18}-Mel and exposed to the dark (minimal lysis) or 525 nm LEDs (66 ± 12% hemolysis relative to Triton X-100 treated RBCs). **Dark/660 nm** (white bars) are RBCs containing surface-anchored C_{18}-Cbl-Cy5BS/C_{18}-Mel and exposed to the dark (minimal lysis) or 660 nm LEDs (66 ± 2% hemolysis relative to Triton X-100 treated RBCs). **660 nm** exposed RBCs containing either C_{18}-Cbl-BS/C_{18}-Mel (black bar) or C_{18}-Cbl-Cy5BS/C_{18}-Mel (white bar). Only the Cy5-containing photolytic trigger responds to 660 nm light. **b.** Confocal microscopy was employed to photohemolyze RBCs in a spatially resolved fashion. The RBCs were internally loaded with BSA-Alexa Fluor 647, so that they could be imaged (at 635 nm) without inducing hemolysis. Photohemolysis (region of illumination outlined in green) was performed using the onboard 515 nm laser. The images by column (left to right) are prephotolysis, a single illumination scan (10 μs/pixel), and three illumination scans. Top row: **Surface Unmodified** control lacks the phototrigger required for hemolysis. As expected, in the absence of the phototrigger, no RBC hemolysis is observed. Middle row: **C_{18}-Cbl-BS** control lacks C_{18}-Mel. As anticipated, in the absence of a functional phototrigger, no RBC hemolysis is observed. Bottom row: RBCs surface modified with the functional phototrigger, **C_{18}-Mel/C_{18}-Cbl-BS**, upon exposure to 515 nm, suffer hemolysis. By contrast, those RBCs outside of the illuminated area are unaffected. Scale bar represents 50 μm. **c.** Assessment of photohemolysis as a function of laser power. RBCs that are not surface loaded with the photolytic trigger (**Surface Unmodified**) do not undergo lysis as assessed by fluorescence of the RBCs in the nonilluminated (red) and illuminated (black, 515 nm, 3X 80% laser power) regions. RBCs surface modified with only **C_{18}-Cbl-BS** likewise do not lyse in response to 515 illumination. By contrast, RBCs containing both **C_{18}-Cbl-BS/C_{18}-Mel** undergo robust hemolysis upon exposure to 515 nm at high (black, 3X 80% laser power), medium (dark gray, 1X 80% laser power), and low (light gray, 1X 10% laser power) illumination conditions. **d.** Liposomes internally loaded with fluorescently quenched 5(6)-carboxyfluorescein were surface modified with C_{18}-Mel/C_{18}-Cbl-BS (purple) or C_{18}-Cbl-BS alone (gray) and subsequently exposed to 494 nm in a spectrofluorimeter to furnish both photolysis and a fluorescent readout of 5(6)-carboxyfluorescein. Controls include liposomes directly treated with C_{18}-Mel (red) and liposomes with no surface modification (green).

trigger. Mel is biosynthesized in honeybees as promelittin, a nonhemolytic peptide comprised of the positively charged Mel and a negatively charged inhibitory prodomain [Blocking Segment (BS)].[25,26] We chemically synthesized Mel and BS as separate modified peptides (Figure 1b). The photohemolytic trigger is comprised of two entities: (1) Mel acylated at its N-terminus with stearic acid (C_{18}). The stearyl lipid moiety of C_{18}-Mel is employed to anchor Mel to the surface of RBCs. (2) The BS is covalently appended to a butyric acid linker, which, in turn, is attached to the Co of a C_{18}-modified Cbl (C_{18}-Cbl-BS; Figure 1c, Schemes S1−S3). We found that RBCs exposed to a premixed combination of C_{18}-Mel and C_{18}-Cbl-BS at a ratio of 1:2 do not undergo hemolysis (Figure 1d). As an aside, we note that the K_D for the Mel/BS complex (SI Figure S8) is 15.2 ± 2.6 μM via isothermal calorimetry. However, this value undoubtedly underestimates the effective K_D once both peptides are bound to the two-dimensional RBC surface. Using a derivative of C_{18}-Cbl-BS with a Cy5 fluorophore (Scheme S4, C_{18}-Cbl-Cy5BS), we were able to quantify the number of C_{18}-Mel molecules on the surface of the RBCs (~6×10^6 molecules/RBC). This is in agreement with previous reports of the maximum loading of melittin molecules as 1.8×10^7 molecules/RBC during hemolysis.[27] Upon illumination, the Co−C bond of C_{18}-Cbl-BS is designed to undergo photocleavage, releasing the BS peptide from the RBC surface,

https://dx.doi.org/10.1021/acscentsci.0c01151
ACS Cent. Sci. 2021, 7, 93−103

exposing free Mel, inducing RBC lysis, and thereby liberating the internally loaded protein contents (Figure 1d).

Our initial studies explored the release of bovine serum albumin-Texas Red (BSA-TxRed) from human RBCs. Internal loading of BSA-TxRed into RBCs was performed under hypotonic conditions in the presence of 60 μM BSA, which was confirmed via flow cytometry and confocal microscopy (Figure S9). Under these conditions, we achieved a loaded internal BSA concentration of 20 ± 2 μM. Light-triggered BSA-TxRed/RBC hemolysis was quantified via the release of fluorescence into the supernatant (Figure 2a). The results were compared relative to RBCs that lack the surface-anchored photolytic trigger (Surface Unmodified) and RBCs that were completely lysed by detergent (Triton X-100). These controls set the minimum and maximum supernatant fluorescence, respectively. Minimal fluorescence (which is taken as minimal lysis) is observed when the RBC membrane contains only C_{18}-Cbl-BS or C_{18}-Cbl-Cy5BS. These results demonstrate that C_{18}-Mel is essential for hemolysis. In addition, RBCs containing both C_{18}-Mel and C_{18}-Cbl-BS (or C_{18}-Cbl-Cy5BS) without light exposure (Dark) likewise display minimal lysis, thereby demonstrating a dependence on light for hemolysis. Finally, surface coloading C_{18}-Cbl-BS and C_{18}-Mel onto human RBCs and subsequent exposure to 525 nm light results in hemolysis that is 66 ± 12% of that observed with Triton X-100. Analogous results were acquired using mouse RBCs (Figure S10).

A key challenge in utilizing photosensitive therapeutics is developing compounds that are responsive to wavelengths that can effectively penetrate tissue (600−900 nm), known as the optical window of tissue.[16,23,24,28−32] We have previously shown that the photolytic wavelength can be tuned to the optical window of tissue by appending long-wavelength fluorophores to Cbl.[23,24,29] We explored long wavelength photolysis using a Cy5 derivatized BS peptide (C_{18}-Cbl-Cy5BS; Scheme S4) that absorbs light at 660 nm. We note that, in the absence of the Cy5 fluorophore, RBCs containing C_{18}-Mel and C_{18}-Cbl-BS do not suffer hemolysis upon exposure to 660 nm (Figure 2a). By contrast, RBCs loaded with the Cy5 antenna (C_{18}-Mel/C_{18}-Cbl-Cy5BS) undergo ready 660 nm-triggered lysis (66 ± 2% relative to Triton X-100-treated RBCs). This result suggests that fluorophores can be used to tune the hemolytic sensitivity of RBCs to specific wavelengths, potentially enabling the release of different proteins from different RBC carriers in a wavelength-dependent fashion. High-level spatiotemporal delivery of multiple protein therapeutics is sought after for the treatment of a variety of biomedical indications, including myocardial infarction, bone fractures, rebuilding vascular networks, and tissue regeneration.[30,33]

Light-mediated delivery of therapeutic agents has received significant attention due to the promise of exquisite spatial control.[4,14,16,17,30] We investigated spatially resolved photorelease using RBCs internally loaded with BSA-Alexa Fluor 647 (Figure 2b) and surface modified with C_{18}-Mel and C_{18}-Cbl-BS. We also employed two controls: RBCs surface modified with only C_{18}-Cbl-BS as well as RBCs that are not surface altered. The combination of C_{18}-Mel/C_{18}-Cbl-BS on the surface and BSA-Alexa Fluor 647 in the interior allowed imaging of intact RBCs containing fluorescent BSA (at 635 nm) without triggering hemolysis. We exposed the RBC samples to 515 nm (confocal microscopy) in a spatially well-defined fashion (region of illumination outlined in green. As expected, RBCs lacking the C_{18}-Mel/C_{18}-Cbl-BS trigger retain BSA-Alexa Fluor 647 fluorescence in both the 515 nm illuminated and nonilluminated regions (Figure 2b, top row). Similarly, RBCs surface labeled with C_{18}-Cbl-BS alone are likewise stable to exposure to 515 nm (Figure 2b, middle row), demonstrating that melittin is required to observe hemolysis. Finally, 515 nm-exposed RBCs containing both C_{18}-Cbl-BS and C_{18}-Mel on the surface undergo rapid photohemolysis as evidenced by the loss of internal fluorescence at 635 nm (Figure 2b, bottom row). It is important to note the release of BSA fluorescence is only observed in the region containing cells exposed to 515 nm light, thereby demonstrating that spatially controlled photohemolysis is feasible. In addition, we subjected a subset of these RBCs to illumination at an 8-fold reduced laser power setting (Figure 2c). As expected, photohemolysis is still observed but to a lesser extent than that detected at the higher laser setting. These results are consistent with the notion that light modulation can control both the locus and the extent of protein release.

In addition to RBCs, melittin is capable of binding to and lysing a variety of other lipid membrane-containing species.[20,25,26] To further expand the potential utility of the Mel-based phototrigger, we investigated the controlled photolysis of liposomes. Liposomes have received extensive attention as drug delivery vehicles, and there are numerous liposomal drug formulations used in the clinic.[2,14] In addition, there is keen interest in extending the drug transportation properties of liposomes to include drug delivery by controlling when and where therapeutic agents are released.[2]

We introduced C_{18}-Cbl-BS and C_{18}-Mel onto the surface of liposomes containing internally loaded 5(6)-carboxyfluorescein, which is fluorescently quenched at the 100 mM loading concentration. We also examined several controls, including liposomes that were not surface modified, those containing only C_{18}-Cbl-BS, and liposomes exposed to C_{18}-Mel (Figure 2d). Illumination of liposome/surface unmodified and liposome/C_{18}-Cbl-BS failed to elicit a lytic response. By contrast, exposure of liposomes to C_{18}-Mel generated a robust fluorescent increase, indicative of release of internally loaded 5(6)-carboxyfluorescein. Finally, we illuminated C_{18}-Mel/C_{18}-Cbl-BS surface-modified liposomes and observed a response analogous to that of C_{18}-Mel-treated liposomes. This supports the hypothesis that lipid membrane formulations are susceptible to photodisruption by the photoresponsive Mel-based construct.

Encouraged with the photorelease of fluorescently labeled constructs, we subsequently evaluated the ability of RBCs to load and release proteins that have potential therapeutic utility. Vascular Endothelial Growth Factor-A (VEGF) is a potent pro-angiogenic protein that has received significant therapeutic attention.[34−37] Although therapeutic angiogenesis has been actively pursued as a strategy for the treatment of various cardiovascular diseases, the results of clinical trials have thus far been disappointing.[35−38] This is due, in large part, to the short intravascular lifespan of VEGF (and related therapeutic proteins), which interferes with the ability to achieve effective concentrations at the desired site(s) over a requisite time interval.[36,38]

Human RBCs were exposed to VEGF (1.4 μM) under hypotonic conditions to furnish VEGF-loaded RBCs (1.1 ± 0.3 μM). The RBCs were diluted to a 4% hematocrit and the presence of free VEGF in unlysed (30 ng/mL) and mechanically lysed (1900 ng/mL) RBCs quantified via a

https://dx.doi.org/10.1021/acscentsci.0c01151
ACS Cent. Sci. 2021, 7, 93−103

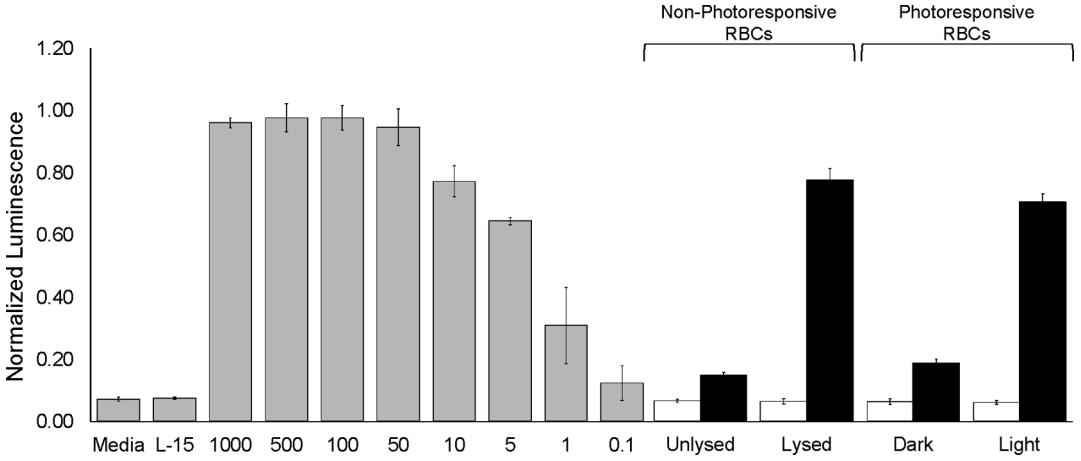

Figure 3. Genetically engineered HEK-293 cells that express luciferase in response to VEGF were exposed to various treatments. HEK-293 cells treated with media or buffer exhibit low luminescence, while cells exposed to recombinant VEGF display a concentration-dependent luminescence (gray bars). HEK-293 cells treated with the supernatants of buffer-loaded RBCs (white bars) which are **Unlysed** or glass-bead **Lysed** RBCs induce negligible luminescence, consistent with the absence of VEGF in the media. Similar nominal luminescence was observed for HEK-293 cells that had been treated with the supernatant of **Unlysed** VEGF-loaded RBCs (black bar). By contrast, glass bead **Lysed** VEGF-loaded RBCs (black bar) induce a significant luminescent response in HEK-293 cells. Finally, we examined the impact of RBCs surface modified with the phototrigger containing either buffer (white bars) or VEGF (black bars). In the **Dark**, the buffer-loaded RBCs (white bars) do not produce a VEGF-dependent luminescent response. The corresponding response in the **Dark** from the VEGF-loaded RBCs is slightly above background (similar to that observed with **Unlysed** VEGF-loaded RBCs) and may be a consequence of the presence of residual unloaded VEGF in solution. By contrast, exposure of RBCs containing VEGF to **Light** triggers a robust luminescence, which is approximately 80-fold greater than that observed with RBCs in the dark.

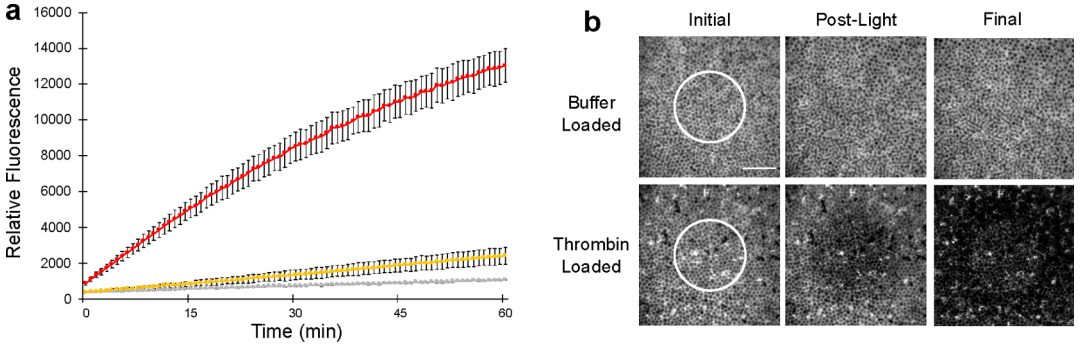

Figure 4. a. Thrombin catalytic activity was assessed using commercially available fluorescent thrombin benzoyl-FVR-(aminomethylcoumarin). Illumination of RBCs internally loaded with thrombin and surface modified with C_{18}-Mel/C_{18}-Cbl-BS (red curve). Unilluminated RBCs internally loaded with thrombin and surface modified with C_{18}-Mel/C_{18}-Cbl-BS (yellow curve). Illumination of thrombin-loaded control lacking the surface modified photolytic trigger (gray curve). Error bars represent standard deviation. **b**. RBCs surface modified with C_{18}-Mel/C_{18}-Cbl-BS were incubated with (Alexa Fluor 647)-fibrinogen and imaged using a confocal microscope. The region of photolysis (photolytic dwell time 10 μs/pixel, 80% power of 515 nm laser) is highlighted prior to (left), immediately after (middle), and 210 s after (right) 515 nm exposure. Surface modified RBCs that were internally buffer-loaded (top row) do not induce conversion of fibrinogen to fibrin. By contrast, thrombin-loaded RBCs that contain the surface phototrigger (bottom row) provoke the formation of an insoluble fibrin gel matrix immediately after photolysis. The fibrin matrix rapidly spreads throughout the field of view within 3.5 min. Scale bar represents 50 μm.

commercial ELISA kit. Analogous studies were performed with VEGF-loaded RBCs that were surface modified with Mel/BS. In the dark, a minimal free VEGF concentration (60 ng/mL) was detected. By contrast, exposure to 525 nm generated a 33-fold increase (2000 ng/mL) in RBC-free VEGF. To ensure the released VEGF is capable of biological activity, we employed a previously described VEGF reporter HEK293 cell line.[34] These cells utilize a luciferase reporter that is under the control of nuclear factor activated T cell response elements. VEGF binding to its receptor (KDR) on the cell surface triggers the expression of luciferase. As expected, buffer-loaded RBCs, whether unlysed or mechanically lysed, elicit a minimal luminescent response analogous to HEK293s treated with media or buffer (Figure 3). Similarly, cells treated with the dark or light exposed, buffer-loaded RBCs containing C_{18}-Mel and C_{18}-Cbl-BS on their surface exhibit nominal luminescence. Finally, RBCs internally loaded with VEGF and surface modified with BS/Mel were either kept in the dark or exposed to 525 nm. As expected, HEK293s treated with RBCs kept in the dark display a low luminescence signal. This is in agreement with the low amount of VEGF present under nonilluminated conditions as established by the ELISA. By contrast, a robust high luminescence readout is observed upon photohemolysis, thereby demonstrating that the photoreleased VEGF is biologically active.

Like VEGF and related angiogenic factors, proteins that disrupt blood flow have also received extensive therapeutic attention. For example, the targeted delivery of Tissue Factor (TF) to tumors has been studied for the treatment of cancer.[39−41] TF promotes blood clotting as a key participant in

https://dx.doi.org/10.1021/acscentsci.0c01151
ACS Cent. Sci. 2021, 7, 93−103

a biochemical cascade that results in the activation of thrombin and the subsequent conversion of soluble fibrinogen to insoluble clot-forming fibrin.[42] Although TF has been explored as an agent designed to starve tumors of their blood supply,[40] the results obtained to date are disappointing due, in large part, to the brief circulatory half-life of TF (<1 min).[43] Thrombin could potentially be used in a fashion analogous to that of TF, but due to potentially devastating systemic side effects, thrombin is currently limited to use as a topical agent to prevent excessive bleeding during surgery.[44] The delivery of potent procoagulant proteins must be carefully controlled since clotting at unwanted sites can lead to deadly side effects such as myocardial infarction or stroke. We sought to determine if controlled delivery of thrombin is capable of forming clots in a spatially well-defined fashion.

RBCs were exposed to a hypotonic solution of thrombin (0.35 μM) to furnish an internally loaded thrombin concentration of 0.17 ± 0.01 μM. The thrombin-loaded RBCs were subsequently surface modified with the photohemolytic C_{18}-Cbl-BS/C_{18}-Mel trigger. We first examined the proteolytic activity of photoreleased thrombin using a fluorescent assay that employs a peptide-based thrombin substrate. Maximum thrombin release was established using C_{18}-Mel as a positive hemolytic control. Based on the latter, photohemolysis releases approximately 50% of total thrombin activity (Figure 4a). By contrast, we observe minimal thrombin activity with RBCs incubated in the dark, which is comparable to the nearly negligible activity detected with RBCs that lack a phototrigger.

We examined spatially directed thrombin photorelease using a fibrin polymerization assay. In brief, thrombin-catalyzed proteolysis of (Alexa Fluor 647)-fibrinogen generates insoluble fibrin, which polymerizes and forms a gel matrix. Both thrombin-loaded and -unloaded RBCs were suspended in solution with fluorescent fibrinogen and imaged using confocal microscopy (Figure 4b). Photoresponsive RBCs containing only buffer were exposed to light (white circle) and, as expected, the fluorescence of the fibrinogen matrix remained unchanged over time. Illumination of thrombin-loaded RBCs that contain only C_{18}-Cbl-BS on the cell surface, likewise, has no impact on fibrinogen matrix fluorescence (Figure S11). By contrast, thrombin-loaded RBCs surface modified with the fully active phototrigger generate the anticipated change that represents the conversion of fibrinogen to polymerized fibrin. This transformation is initially seen only in the region of illumination. However, as expected for a freely diffusing enzyme unleashed in a small delimited region, the spread of polymerized fibrin ultimately encompasses the field of view.

We subsequently examined the light-induced, spatially focused delivery of thrombin *in vivo*. Healthy FVB mice were tail vein injected with either RBCs loaded with thrombin (experimental group) or only buffer (control group). In both cases, the mouse RBCs were surface modified with the functional photohemolytic trigger. For both groups, a single ear was spot illuminated at 561 nm under a confocal microscope using an on-board laser. After light treatment, the animals were sacrificed, and both light and dark exposed ears were collected. The ears were sectioned and subsequently stained with the Martius Scarlet Blue trichrome stain, which specifically labels collagen blue, RBCs yellow, and fibrin red (Figure 5).[45] Mice injected with buffer-only RBCs display minimal fibrin staining in the blood vessels of both the light and dark ears (Figure S12). In addition, minimal fibrin staining

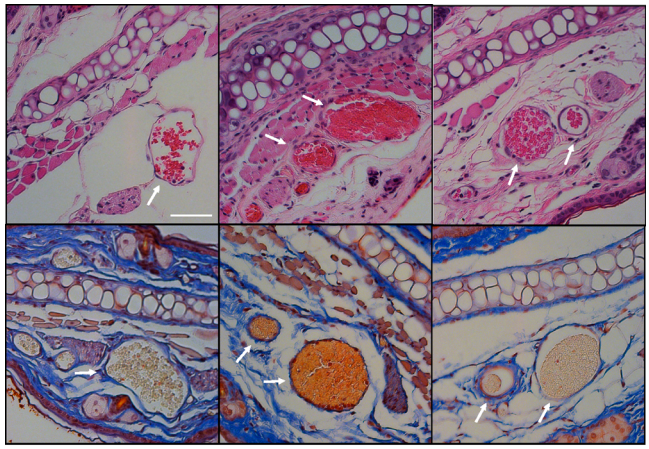

Figure 5. Murine RBCs internally loaded with buffer or thrombin and surface modified with C_{18}-Mel/C_{18}-Cbl-BS were tail vein injected into healthy FVB mice (n = 4 for each experimental condition). A 1 mm^2 region of one ear from each mouse was illuminated (561 nm) under a confocal microscope, the mice were euthanized, and both "dark" and "light" ears were harvested. Four μm cross sections of the fixed tissues were stained with H&E (top row) and Martius Scarlet Blue dyes (bottom row). Left: "Dark" ear reveals healthy blood vessels with RBCs stained yellow (bottom image). Middle: "Light" ear displays the presence of fibrin (orange/red; bottom image) and significant vascular congestion. Right: Light exposed ear from animals injected with photoresponsive RBCs that were internally loaded with buffer. The blood vessels do not display fibrin or venous congestion as evidenced by the free space between the RBCs and the endothelium. Scale bar = 50 μm.

is observed in blood vessels of the nonilluminated ears from mice injected with thrombin-loaded RBCs. By contrast, the vasculature in all of the light exposed ears exhibit a deep red stain indicative of fibrin formation. Statistical analysis revealed there are significant (p-value = 0.0143) thrombin and (p-value = 0.0143) illumination effects on fibrin formation. The vessels in the experimental light exposed ear also possess minimal free space between RBCs and the endothelium, indicative of vascular congestion, which is consistent with clot formation. As expected, no congestion is observed in any of the non-illuminated experimental ears, thereby demonstrating healthy vasculature in spite of the presence of circulating thrombin-containing RBCs. Furthermore, both fibrin formation and vascular congestion are simultaneously observed in all light-treated ears, save for one mouse, which only exhibited fibrin formation. We do note that the absence of congestion does not rule out the formation of a clot, merely the impact of that clot on blood vessel engorgement. Finally, we have determined that the total amount of Mel introduced is 30 μg/mouse, a dose previously shown to be safe, lacking side effects or tissue abnormalities in mice.[46]

SUMMARY

In summary, we have designed a photohemolytic platform capable of releasing proteins from RBCs in response to light. This cell-based delivery system has been validated by loading and releasing three proteins that vary in size (21−66 kDa) and isoelectric point (4.7−7.6). Given the established properties of melittin as a lytic agent for lipid bilayer-based vesicles (exosomes, microvesicles, liposomes, etc.) we anticipate that this strategy could prove useful for the light-triggered release of

https://dx.doi.org/10.1021/acscentsci.0c01151
ACS Cent. Sci. 2021, 7, 93−103

intravesicular contents from a variety of carriers. Finally, we note that therapeutic protein release from a long-lived vascular carrier has potential biomedical implications that include therapeutic angiogenesis, thrombolysis, and antiangiogenesis therapy for the treatment of cancer. These studies are in progress.

EXPERIMENTAL SECTION

Materials. All materials were purchased from Sigma-Aldrich, Fisher Scientific, or VWR unless noted otherwise. Human red blood cells (hRBCs) were purchased from ZenBio. Mice were purchased from Jackson Laboratories.

Internal Loading of hRBCs. 100 μL of hRBCs (less than 3 weeks old) was washed 3−5 times in fresh Leibovitz-15 media and then centrifuged at 1000×g for 3 min at room temperature. The supernatant of the final wash was removed to furnish an RBC pellet, which was diluted with a concentrated protein solution to provide a final hematocrit of 70%. BSA-Fluorophore (BSA-FITC, BSA-Texas Red, or BSA-Alexa Fluor 647) had a final loading concentration of 4.0 mg/mL, bovine thrombin had a final loading of 5 NIH units, and vascular endothelial growth factor-A (VEGF) had a final loading concentration of 50 μg/mL. For mock-loaded hRBCs, 43 μL of 1× PBS was added to the 100 μL hRBC pellet.

The protein-hRBC mixture was added to a prepared dialysis film with MWCO 1 kDa, clipped on both ends, and submerged in a 4 °C solution of 80 mOsm/L PBS+6 mM glucose while gently stirring for 20 min. The dialysis bag was then transferred to a 1× PBS solution at 37 °C for 10 min. The dialysis bag was washed with 900 μL of L-15 to transfer-loaded RBCs to a new vial. The RBCs were washed 4−6 times in fresh L-15 at 1000×g for 3 min at room temperature.

hRBC Mel/BS External Loading. Protein-loaded or mock-loaded hRBCs (see Internal Loading of hRBCs) were diluted to a concentration of 4.0×10^8 cells/mL in L-15 media. C_{18}-Melittin (C_{18}-Mel) was added to a fresh plastic 1.5 mL tube so the final concentration, after the addition of hRBCs, was 20 μM with a 1:2 ratio of C_{18}-Mel:C_{18}-Cbl-BS or a 1:4 ratio of C_{18}-Mel:C18-Cbl-Cy5BS. The mixtures were left in the dark to equilibrate for 10 min. hRBCs were added to the C_{18}-Mel/C_{18}-Cbl-BS or C_{18}-Mel/C_{18}-Cbl-Cy5BS solution and incubated for 30 min in the dark. The photoresponsive hRBCs were then washed 1−2 times by centrifuging 1000×g for 3 min and replacing supernatant with fresh L-15.

Mouse Red Blood Cell (mRBC) Collection and Isolation. Whole blood was collected from FVB mice via cardiac puncture on the same day the mRBCs were scheduled to be used. The whole blood was diluted 1:3 with 2 mM EDTA in 1× DPBS. Four mL of whole blood was carefully pipetted to the top layer of 3 mL of sterile Ficoll-Paque Premium. The blood-Ficoll mixture was centrifuged for 30 min at 400×g. The mRBCs were then collected and washed with 1× PBS 3−5 times by centrifuging at 600×g for 2 min at 4 °C

Internal Loading of mRBCs. 200−600 μL of mRBCs (see mRBC Collection and Isolation) was prepared in a single dialysis bag (MWCO 1 kDa) and was diluted with a concentrated protein solution to provide a final hematocrit of 70%. BSA-Fluorophore (BSA-FITC or BSA-Texas Red) had a final loading concentration of 4.0 mg/mL, and bovine thrombin had a final loading of 5 NIH units. For mock-loaded mRBCs, 1× PBS was added to the mRBCs so the final hematocrit was 70%.

The protein/mRBC mixture was added to a prepared dialysis film with MWCO 1 kDa, clipped on both ends, and submerged in a 4 °C solution of 80 mOsm/L PBS, 10 mM glucose, 0.25% glycerol, and 2 mM ATP (added the day of loading) while stirring gently for 40 min. Cells were recovered from the dialysis bags with a small amount of 1× PBS (less than 400 μL) and added to a fresh plastic 1.5 mL tube. The solutions were brought to isotonic conditions with 10× PBS and then incubated at 37 °C for 20 min. The mRBCs were washed 4−6 times in fresh 1× PBS at 600×g for 2 min at 4 °C.

mRBC Mel/BS External Loading. 100 μL of protein-loaded or mock-loaded mRBCs (see Internal Loading of mRBCs) was diluted to a 10% hematocrit in 1× PBS. Enough C_{18}-Mel was added to a fresh plastic 1.5 mL tube so the final concentration after the addition of mRBCs was 20 μM with a 1:2 ratio of C_{18}-Mel:C_{18}-Cbl-BS and left in the dark to equilibrate for 10 min. The mRBCs were added to the C_{18}-Mel/C_{18}-Cbl-BS solution and incubated for 30 min in the dark. The photoresponsive mRBCs were then centrifuged at 600×g for 2 min, and the supernatant was removed.

Photoresponsive RBC Lysis Assay. 100 μL of 4.0×10^8 photoresponsive RBCs/mL internally loaded with BSA-Texas Red (see hRBC Mel/BS External Loading) was added to individual plastic 1.5 mL tubes containing 125 μL of L-15 or 125 μL of 1% Triton X-100 (positive control). Tubes were then incubated in the dark or under an LED board at 525 or 660 nm for 30 min. Cells were spun down for 3 min at 1000×g, and supernatants were collected. The fluorescence was measured at Ex/Em 596/615 nm to determine release of BSA-Texas Red. BSA-Texas Red-hRBCs that were not surface modified with C_{18}-Mel/C_{18}-Cbl-BS were illuminated for 30 min and used as a negative control. The fluorescence of L-15 alone was used as a blank control. Percent lysis was determined by the following equation:

$$(\text{Fluorescence}_{\text{sample}} - \text{Fluorescence}_{\text{Blank}}) / (\text{Fluorescence}_{\text{positive}} - \text{Fluorescence}_{\text{Blank}})$$

Thrombin Activity Assay. 100 μL of 4.0×10^8 photoresponsive RBCs/mL internally loaded with thrombin (see hRBC Mel/BS External Loading) was added to individual plastic 1.5 mL tubes containing 125 μL of L-15 or 125 μL of 20 μM Mel (positive control). Tubes were then incubated in the dark or under an LED board at 525 nm for 30 min. Cells were spun down for 3 min at 1000×g, and supernatants were collected. An aliquot from each supernatant (20 μL) was added to reaction mixtures with spiked thrombin ranging from 0 to 0.5 Units/mL, 10 μM thrombin Fluorogenic Substrate III (Calbiochem, benzoyl-FVR-[aminomethyl coumarin]), and 100 mM Tris pH 8.0 buffer. The fluorescence at Ex/Em of 370/450 nm of these samples was measured every 45 s for 2 h. Standard addition curves were constructed to determine the activity of thrombin in each sample (Figure S13).

hRBC/VEGF ELISA. 100 μL of 4.0×10^8 photoresponsive RBCs/mL internally loaded with VEGF (see hRBC Mel/BS External Loading) was added to individual plastic 1.5 mL tubes. Tubes were then incubated in the dark or under an LED board at 525 nm for 30 min. Cells were spun down for 3 min at 1000×g, and supernatants were collected and diluted 100−10,000 fold with L-15. VEGF-hRBCs and Mock-hRBCs that were not surface modified with C_{18}-Mel/C_{18}-Cbl-BS were illuminated for 30 min and used as a negative control or vortexed with shredder beads and used as a positive lysis

https://dx.doi.org/10.1021/acscentsci.0c01151
ACS Cent. Sci. 2021, 7, 93−103

control. An ELISA plate and standards (Invitrogen BMS277-2) were prepared following the manufacturer's protocol, and the concentration of VEGF in each sample was determined using a standard curve (Figure S14).

VEGF Reporter Cells Activity Assay. 100 μL of 4.0×10^8 photoresponsive RBCs/mL internally loaded with VEGF or internally mock loaded (see hRBC Mel/BS External Loading) was added to individual plastic 1.5 mL tubes. Tubes were then incubated in the dark or under an LED board at 525 nm for 30 min. Cells were spun down for 3 min at 1000×g, and supernatants were collected and 10-fold diluted with 10% FBS in Dulbecco's Modified Eagle's Medium (DMEM). VEGF-hRBCs and Mock-hRBCs that were not surface modified with C_{18}-Mel/C_{18}-Cbl-BS were illuminated for 30 min and used as a negative control or vortexed with shredder beads and used as a positive lysis control. Both positive and negative controls were 10-fold diluted with 10% FBS in DMEM. "Thaw-and-use" VEGF Bioassay Cells (KDR/NFAT-RE HEK293 cells, Promega GA2001) were thawed and plated following the manufacturer's protocol. Plated cells were immediately treated with full media, L-15, pure VEGF protein, or the supernatants from the hRBC samples prepared above following the manufacturer's protocol. Plates were incubated in a 37 °C, 5% CO_2 incubator for 6 h. Following incubation, cells were treated with supplied Bio-Glo reagent, and the luminescence of each well was measured following the manufacturer's instructions.

Liposome Kinetic Assay. Custom DOPC:DOPE liposomes were purchased from Encapsula Nanosciences containing 100 mM 5(6)-carboxyfluorescein and a total lipid concentration of 10 mM. Prior to each experiment, excess 5(6)-carboxyfluorescein was removed from the liposomes using illustra Microspin G-50 columns. The columns were prepared according to the manufacturer's instructors, and 10 μL of liposomes was sent through the column. The cleaned liposomes were diluted 100× with L-15. Samples were prepared with 10 μM C_{18}-Mel, 30 μM C_{18}-Cbl-BS, 10 μM C_{18}-Mel, and 30 μM C_{18}-Cbl-BS (adding the liposomes last) or just L-15. Fluorescence kinetics was acquired in a spectrofluorimeter using 494 nm, which is absorbed by both Cbl (to enable lysis) and the freed unquenched 5(6)-carboxyfluorescein (l_{em} = 515 nm). Data was collected every second for 8 min.

Mel/BS Loading Concentration Assay. Mock-loaded hRBCs were surface modified with C_{18}-Cbl-Cy5BS as described in hRBC Mel/BS External Loading. The hRBCs (n = 3) were 10× diluted to a final concentration of 0.1% Triton and exposed to 525 nm light for 1 h to ensure photolysis of the Cy5-BS peptide. The absorbance at 646 nm of the supernatant of these samples was measured to determine the amount of C_{18}-Cbl-Cy5-BS that was installed on the surface of hRBCs. Mock-loaded hRBCs (not surface modified with C_{18}-Cbl-Cy5-BS) were used as a blank, and pure C_{18}-Cbl-Cy5-BS was used to determine the extinction coefficient of the photolyzed BS peptide.

Isothermal Calorimetry. Automated isothermal calorimetry (ITC) experiments were conducted using the MiroCal Auto-iTC200 instrument. Pure melittin (Mel) peptide (100 μM) in L-15 was used in the cell, and 1.5 mM of pure BlockingSegment (BS) peptide in L-15 was used in the syringe as the ligand. The cell was set to 26 °C and had a stirring speed of 750 rpm. The reference power was 8 μCal/s, and 20 injections took place 180 s apart.

Confocal Microscopy. All imaging was performed on an inverted Olympus FV1000 scanning confocal microscope with an IX81 base. DiO, BSA-TexasRed and BSA-Alexa Fluor 647 were imaged with 488, 559, and 635 nm laser lines, respectively. Photolysis was performed using a 10 mW 515 nm laser line at 10−80% maximal power for indicated durations of photolysis at 10−100 μs/pixel dwell time.

Flow Cytometry Analysis. Flow cytometry analysis was conducted on a Thermo Fisher Attune NxT using the equipped 488 and 561 nm lasers for analysis of DiO and BSA-Texas Red, respectively. A scatter plot of aspect ratio/area was used to gate for single cells, and the remaining cells were plotted on a DiO fluorescence intensity versus Texas Red fluorescence intensity scatter plot.

Imaging DiO/TxRed-BSA-Loaded RBCs. hRBCs were internally loaded with BSA-Texas Red as described in Internal Loading of hRBCs. A subset of BSA-Texas Red hRBCs in 0.02% fetal bovine serum (FBS) L-15 at a 10% hematocrit was then surface modified with DiO by incubating with 25 μM of DiO at 37 °C for 45 min. DiO/BSA-Texas Red-loaded RBCs were analyzed as described in Flow Cytometry Analysis and imaged on the confocal microscope described in Confocal Microscopy with a 100× oil objective. Imaging was performed with 1024 × 1024 pixel resolution and 1.3× zoom with a 10 μs/pixel dwell time and 4× Kalman averaging by line. The DiO and TexasRed channels were excited by 488 and 559 laser lines respectively and imaged sequentially to minimize spectral bleed-through.

Photolytic Release of BSA-Alexa Fluor 647 from Loaded RBCs. RBCs loaded with BSA-Alexa Fluor 647 and C_{18}-Mel/C_{18}-Cbl-BS (see hRBC Mel/BS External Loading) were pipetted into channels of ibidi μ-slide VI 0.5 glass bottom slides coated with poly-L-lysine (Sigma) and equilibrated in the dark on the microscope for 5−10 min before imaging. The final RBC hematocrit was 1%. Images were acquired every 10 s. A single image was acquired before photolysis commenced followed by 6 additional frames after photolysis. The photolysis region of interest (ROI) was defined to be the middle third of the field of view. Image analysis was performed in imageJ. Relative fluorescent intensity was calculated by dividing the mean fluorescent intensity of an ROI at time x by the mean fluorescent intensity at time 0.

Fibrin Gel Assay. Alexa Fluor 647 conjugated fibrinogen (ThermoFisher) was reconstituted to 3 mg/mL in 0.1 M $NaHCO_3$ according to the manufacturer's instructions. RBC free fibrin assays were performed at an Alexafluor 647-fibrinogen concentration of 1 mg/mL in fibrinogen assay buffer composed of 50 mM Tris pH 7.5, 0.1 M NaCl, and 20 mM $CaCl_2$. The fluorescent fibrinogen solution was initially plated on a glass bottom 35 mm dish (Mattek #1.5 glass coverslip) and imaged on the confocal microscope described in Confocal Microscopy. Thrombin was added to a final concentration of 0.05 U/μL and imaged 1 min later to assess the formation of fluorescent fibrin gel.

Photolytic Release of Thrombin from Loaded RBCs and Subsequent Fibrin Gel Formation. RBCs were internally loaded with thrombin and surface modified with C_{18}-Mel/C_{18}-Cbl-BS as described in hRBC Mel/BS External Loading. A 1% hematocrit suspension of loaded RBCs was made in L-15 media containing 1 mg/mL Alexa Fluor 647 conjugated fibrinogen (ThermoFisher). The suspension was loaded into ibidi μ-slides as described in Photolytic Release of BSA-Alexa Fluor 647 from Loaded RBCs. The suspensions

https://dx.doi.org/10.1021/acscentsci.0c01151
ACS Cent. Sci. 2021, 7, 93−103

were allowed to equilibrate in the dark for 5−10 min before imaging on the confocal microscope described in Confocal Microscopy. Images were acquired in a 512 × 512 pixel window with a 60× oil immersion objective and a dwell time of 10 μs/pixel. Z stacks were acquired at 1.34 μm intervals for a total of ten optical sections spanning 13.4 μm. Stacks were acquired in a time course where one full set of stacks was acquired, photolysis was performed, and nine more sets of stacks followed. Photolysis was performed in a 250 × 250 pixel circular ROI at 80% 515 nm laser power for a total of 6 s.

In Vivo Thrombin Release. Healthy FVB mice were housed in an approved Division of Comparative Medicine facility until time of injection. Mice were anesthetized with 2% isoflurane and placed on a heated stage (37 °C) to maintain their core body temperature throughout the experiment. Hair was removed from both ears using hair removal cream, and the right ear was immobilized by two-sided tape on an aluminum block. Blood vessels were located using the green fluorescence channel on an Olympus IV-100 laser scanning confocal microscope, which was also utilized as a light source for mRBC activation. Prior to injection, mRBCs were mock loaded, BSA-Texas Red loaded, or thrombin loaded as described in Internal Loading of mRBCs. Mock-loaded and thrombin-loaded mRBCs were then surface modified with C_{18}-Mel and C_{18}-Cbl-BS as described in mRBC Mel/BS External Loading. Mice were injected with 30 μL of mRBCs-BSA-Texas Red, 13 μL of 1× PBS, and 100 μL of either mRBCs-thrombin-Mel/BS (thrombin group, n = 4) or mRBCs-Mock-Mel/BS (Mock group, n = 4). The right ear of each mouse was then illuminated with a 488 nm laser at 30% intensity and a 561 nm laser at 45% intensity for 10 min. After 90 min, mice were euthanized with CO_2 followed by a secondary physical method, and both ears were harvested. The animals did not display any signs of distress during the experimental time period. All animal experimentation performed was approved by the Institutional Animal Care and Use Committee at the University of North Carolina at Chapel Hill.

Histology Staining and Imaging. After collection of mouse ears (see In Vivo Thrombin Release), the illuminated blood vessels in the right ears and the corresponding vessels in the nonilluminated ears were marked with a tissue staining dye. All ears were immediately placed in a 10% neutral buffered formalin solution for at least 48 h at room temperature. After fixation, the tissues were placed in a 70% ethanol solution and embedded in paraffin. Tissue cross sections (4 μm) were stained with H&E and Martius Scarlet Blue dyes. Images were acquired using an Olympus BX51 microscope with a 40× objective.

Statistical Analysis of Tissue Images. All MSB stained tissue images in Figure 5 and Figure S12 for the thrombin-light, thrombin-dark, and buffer-light groups were randomized and blinded. A lab member was shown the buffer-dark images as a negative control and was asked two questions: (1) compared to the negative control images, is there fibrin present in the blood vessels, as indicated by the presence of red staining and (2) compared to the negative control images, is there venous congestion present in the blood vessels, as indicated by little spacing between the red blood cells and vessel wall. The lab member answered Yes or No to each question for each image. On the basis of these responses, we calculated the probability of observing a given pattern of outcomes if the null hypothesis (e.g., there is no drug effect) is correct. We reject the null hypothesis and claim the alternative hypothesis (e.g., there is drug effect) to be correct, if this probability for the null hypothesis is small (e.g., <0.05). For example, to test whether there is a drug effect on fibrin formation, we identified that images of 4 (out of 8) mice contain fibrin. If there is no drug effect, the probability that all 4 mice are drug treated is 0.0143 (1/70), and thus we claim that there is a drug effect on fibrin formation. Furthermore, the probability that all 4 images correspond to illuminated ears is 0.0143 (1/70). We, therefore, claim that there is a drug + illumination effect (versus drug + dark effect) on fibrin formation.

Safety Statement. No unexpected or unusually high safety hazards were encountered.

■ ASSOCIATED CONTENT

Supporting Information

The Supporting Information is available free of charge at https://pubs.acs.org/doi/10.1021/acscentsci.0c01151.

Descriptions of synthesis and characterization of peptides and peptide-cobalamin constructs, as well as *in vitro* and *in vivo* analysis of photoresponsive RBCs loaded with protein therapeutics (PDF)

■ AUTHOR INFORMATION

Corresponding Author

David. S. Lawrence − *Department of Chemistry, Division of Chemical Biology and Medicinal Chemistry, Department of Chemistry, and Department of Pharmacology and Department of Chemistry, University of North Carolina, Chapel Hill, North Carolina 27599, United States;* orcid.org/0000-0002-0901-1617; Email: lawrencd@email.unc.edu

Authors

Brianna M. Vickerman − *Department of Chemistry, University of North Carolina, Chapel Hill, North Carolina 27599, United States*

Colin P. O'Banion − *Division of Chemical Biology and Medicinal Chemistry, Department of Chemistry, University of North Carolina, Chapel Hill, North Carolina 27599, United States*

Xianming Tan − *Department of Biostatistics, Lineberger Comprehensive Cancer, Center University of North Carolina at Chapel Hill, Chapel Hill, North Carolina 27599, United States*

Complete contact information is available at: https://pubs.acs.org/10.1021/acscentsci.0c01151

Notes

The authors declare no competing financial interest.

■ ACKNOWLEDGMENTS

We are pleased to acknowledge the Eshelman Institute for Innovation for funding. B.M.V. thanks the American Heart Association for a predoctoral fellowship (18PRE33960038). All animal experimental protocols were approved by the University of North Carolina at Chapel Hill Institutional Animal Care and Use Committee (19-050.0).

■ REFERENCES

(1) Anselmo, A. C.; Gokarn, Y.; Mitragotri, S. Non-invasive delivery strategies for biologics. *Nat. Rev. Drug Discovery* **2019**, *18* (1), 19−40.

(2) Pisal, D. S.; Kosloski, M. P.; Balu-Iyer, S. V. Delivery of therapeutic proteins. *J. Pharm. Sci.* **2010**, *99* (6), 2557−2575.
(3) Rehman, K.; Hamid Akash, M. S.; Akhtar, B.; Tariq, M.; Mahmood, A.; Ibrahim, M. Delivery of Therapeutic Proteins: Challenges and Strategies. *Curr. Drug Targets* **2016**, *17* (10), 1172−1188.
(4) Lu, Y.; Sun, W.; Gu, Z. Stimuli-responsive nanomaterials for therapeutic protein delivery. *J. Controlled Release* **2014**, *194*, 1−19.
(5) Leuzzi, V.; Rossi, L.; Gabucci, C.; Nardecchia, F.; Magnani, M. Erythrocyte-mediated delivery of recombinant enzymes. *J. Inherited Metab. Dis.* **2016**, *39* (4), 519−530.
(6) Josephs, S. F.; Ichim, T. E.; Prince, S. M.; Kesari, S.; Marincola, F. M.; Escobedo, A. R.; Jafri, A. Unleashing endogenous TNF-alpha as a cancer immunotherapeutic. *J. Transl. Med.* **2018**, *16* (1), 242.
(7) Gurewich, V. Therapeutic Fibrinolysis: How Efficacy and Safety Can. Be Improved. *J. Am. Coll. Cardiol.* **2016**, *68* (19), 2099−2106.
(8) Villa, C. H.; Pan, D. C.; Zaitsev, S.; Cines, D. B.; Siegel, D. L.; Muzykantov, V. R. Delivery of drugs bound to erythrocytes: new avenues for an old intravascular carrier. *Ther. Delivery* **2015**, *6* (7), 795−826.
(9) Patel, A.; Patel, M.; Yang, X.; Mitra, A. K. Recent advances in protein and Peptide drug delivery: a special emphasis on polymeric nanoparticles. *Protein Pept. Lett.* **2014**, *21* (11), 1102−1120.
(10) Ding, S.; O'Banion, C. P.; Welfare, J. G.; Lawrence, D. S. Cellular Cyborgs: On the Precipice of a Drug Delivery Revolution. *Cell Chem. Biol.* **2018**, *25* (6), 648−658.
(11) Magnani, M.; Rossi, L. Approaches to erythrocyte-mediated drug delivery. *Expert Opin. Drug Delivery* **2014**, *11* (5), 677−687.
(12) Bourgeaux, V.; Lanao, J. M.; Bax, B. E.; Godfrin, Y. Drug-loaded erythrocytes: on the road toward marketing approval. *Drug Des., Dev. Ther.* **2016**, *10*, 665−676.
(13) Muzykantov, V. R. Drug delivery by red blood cells: vascular carriers designed by mother nature. *Expert Opin. Drug Delivery* **2010**, *7* (4), 403−427.
(14) Mi, P. Stimuli-responsive nanocarriers for drug delivery, tumor imaging, therapy and theranostics. *Theranostics* **2020**, *10* (10), 4557−4588.
(15) Timko, B. P.; Dvir, T.; Kohane, D. S. Remotely triggerable drug delivery systems. *Adv. Mater.* **2010**, *22* (44), 4925−4943.
(16) Shim, G.; Ko, S.; Kim, D.; Le, Q. V.; Park, G. T.; Lee, J.; Kwon, T.; Choi, H. G.; Kim, Y. B.; Oh, Y. K. Light-switchable systems for remotely controlled drug delivery. *J. Controlled Release* **2017**, *267*, 67−79.
(17) Zhou, Y.; Ye, H.; Chen, Y.; Zhu, R.; Yin, L. Photoresponsive Drug/Gene Delivery Systems. *Biomacromolecules* **2018**, *19* (6), 1840−1857.
(18) Yang, Y.; Mu, J.; Xing, B. Photoactivated drug delivery and bioimaging. *Wiley Interdiscip Rev. Nanomed Nanobiotechnol* **2017**, *9* (2), No. e1408.
(19) Raghuraman, H.; Chattopadhyay, A. Melittin: a membrane-active peptide with diverse functions. *Biosci. Rep.* **2007**, *27* (4−5), 189−223.
(20) Memariani, H.; Memariani, M.; Shahidi-Dadras, M.; Nasiri, S.; Akhavan, M. M.; Moravvej, H. Melittin: from honeybees to superbugs. *Appl. Microbiol. Biotechnol.* **2019**, *103* (8), 3265−3276.
(21) Hughes, R. M.; Marvin, C. M.; Rodgers, Z. L.; Ding, S.; Oien, N. P.; Smith, W. J.; Lawrence, D. S. Phototriggered Secretion of Membrane Compartmentalized Bioactive Agents. *Angew. Chem., Int. Ed.* **2016**, *55* (52), 16080−16083.
(22) Shell, T. A.; Lawrence, D. S. Vitamin B12: a tunable, long wavelength, light-responsive platform for launching therapeutic agents. *Acc. Chem. Res.* **2015**, *48* (11), 2866−2874.
(23) Shell, T. A.; Shell, J. R.; Rodgers, Z. L.; Lawrence, D. S. Tunable visible and near-IR photoactivation of light-responsive compounds by using fluorophores as light-capturing antennas. *Angew. Chem., Int. Ed.* **2014**, *53* (3), 875−878.
(24) Smith, W. J.; Oien, N. P.; Hughes, R. M.; Marvin, C. M.; Rodgers, Z. L.; Lee, J.; Lawrence, D. S. Cell-mediated assembly of phototherapeutics. *Angew. Chem., Int. Ed.* **2014**, *53* (41), 10945−10948.
(25) Jallouk, A. P.; Palekar, R. U.; Marsh, J. N.; Pan, H.; Pham, C. T.; Schlesinger, P. H.; Wickline, S. A. Delivery of a Protease-Activated Cytolytic Peptide Prodrug by Perfluorocarbon Nanoparticles. *Bioconjugate Chem.* **2015**, *26* (8), 1640−1650.
(26) LeBeau, A. M.; Brennen, W. N.; Aggarwal, S.; Denmeade, S. R. Targeting the cancer stroma with a fibroblast activation protein-activated promelittin protoxin. *Mol. Cancer Ther.* **2009**, *8* (5), 1378−1386.
(27) Tosteson, M. T.; Holmes, S. J.; Razin, M.; Tosteson, D. C. Melittin lysis of red cells. *J. Membr. Biol.* **1985**, *87* (1), 35−44.
(28) Jaque, D.; Martinez Maestro, L.; del Rosal, B.; Haro-Gonzalez, P.; Benayas, A.; Plaza, J. L.; Martin Rodriguez, E.; Garcia Sole, J. Nanoparticles for photothermal therapies. *Nanoscale* **2014**, *6* (16), 9494−9530.
(29) Marvin, C. M.; Ding, S.; White, R. E.; Orlova, N.; Wang, Q.; Zywot, E. M.; Vickerman, B. M.; Harr, L.; Tarrant, T. K.; Dayton, P. A.; Lawrence, D. S. On Command Drug Delivery via Cell-Conveyed Phototherapeutics. *Small* **2019**, *15* (37), No. 1901442.
(30) Rapp, T. L.; DeForest, C. A. Visible Light-Responsive Dynamic Biomaterials: Going Deeper and Triggering More. *Adv. Healthcare Mater.* **2020**, *9* (7), No. 1901553.
(31) Vorobev, A. Y.; Moskalensky, A. E. Long-wavelength photoremovable protecting groups: On the way to in vivo application. *Comput. Struct. Biotechnol. J.* **2020**, *18*, 27−34.
(32) Tong, R.; Kohane, D. S. Shedding light on nanomedicine. *Wiley Interdiscip Rev. Nanomed Nanobiotechnol* **2012**, *4* (6), 638−662.
(33) Rambhia, K. J.; Ma, P. X. Controlled drug release for tissue engineering. *J. Controlled Release* **2015**, *219*, 119−128.
(34) Wang, L.; Xu, G. L.; Gao, K.; Wilkinson, J.; Zhang, F.; Yu, L.; Liu, C. Y.; Yu, C. F.; Wang, W. B.; Li, M.; Chen, W.; Fan, F.; Cong, M.; Wang, J. Z. Development of a robust reporter-based assay for the bioactivity determination of anti-VEGF therapeutic antibodies. *J. Pharm. Biomed. Anal.* **2016**, *125*, 212−218.
(35) Deveza, L.; Choi, J.; Yang, F. Therapeutic angiogenesis for treating cardiovascular diseases. *Theranostics* **2012**, *2* (8), 801−814.
(36) Chu, H.; Wang, Y. Therapeutic angiogenesis: controlled delivery of angiogenic factors. *Ther. Delivery* **2012**, *3* (6), 693−714.
(37) Melincovici, C. S.; Bosca, A. B.; Susman, S.; Marginean, M.; Mihu, C.; Istrate, M.; Moldovan, I. M.; Roman, A. L.; Mihu, C. M. Vascular endothelial growth factor (VEGF) - key factor in normal and pathological angiogenesis. *Rom. J. Morphol. Embryol.* **2018**, *59* (2), 455−467.
(38) Van Hove, A. H.; Benoit, D. S. Depot-Based Delivery Systems for Pro-Angiogenic Peptides: A Review. *Front. Bioeng. Biotechnol.* **2015**, *3*, 102.
(39) Eisenreich, A.; Bolbrinker, J.; Leppert, U. Tissue Factor: A Conventional or Alternative Target in Cancer Therapy. *Clin. Chem.* **2016**, *62* (4), 563−570.
(40) Shi, Q.; Zhang, Y.; Liu, S.; Liu, G.; Xu, J.; Zhao, X.; Anderson, G. J.; Nie, G.; Li, S. Specific tissue factor delivery using a tumor-homing peptide for inducing tumor infarction. *Biochem. Pharmacol.* **2018**, *156*, 501−510.
(41) Shi, W.; Mei, H.; Deng, J.; Chen, C.; Wang, H.; Guo, T.; Zhang, B.; Li, L.; Pang, Z.; Jiang, X.; Shen, S.; Hu, Y. A tissue factor targeted nanomedical system for thrombi-specific drug delivery. *Biomaterials* **2012**, *33* (30), 7643−7654.
(42) Grover, S. P.; Mackman, N. Tissue Factor: An Essential Mediator of Hemostasis and Trigger of Thrombosis. *Arterioscler., Thromb., Vasc. Biol.* **2018**, *38* (4), 709−725.
(43) Brand, C.; Dencks, S.; Schmitz, G.; Muhlmeister, M.; Stypmann, J.; Ross, R.; Hintelmann, H.; Schliemann, C.; Muller-Tidow, C.; Mesters, R. M.; Berdel, W. E.; Schwoppe, C. Low-Energy Ultrasound Treatment Improves Regional Tumor Vessel Infarction by Retargeted Tissue Factor. *J. Ultrasound Med.* **2015**, *34* (7), 1227−1236.

https://dx.doi.org/10.1021/acscentsci.0c01151
ACS Cent. Sci. 2021, 7, 93−103

(44) Lundblad, R. L.; Bradshaw, R. A.; Gabriel, D.; Ortel, T. L.; Lawson, J.; Mann, K. G. A review of the therapeutic uses of thrombin. *Thromb. Haemostasis* **2004**, *91* (5), 851−860.
(45) Lendrum, A. C.; Fraser, D. S.; Slidders, W.; Henderson, R. Studies on the character and staining of fibrin. *J. Clin. Pathol.* **1962**, *15*, 401−413.
(46) Khalil, E. A. G.; Saeed, W. S. E. Toxic Effects and Safety of Bee Venom Protein [Melittin] in Mice: Search for Natural Vaccine Adjuvants. *J. Nat. Prod. Resour.* **2017**, *3* (1), 111−114.

https://dx.doi.org/10.1021/acscentsci.0c01151
ACS Cent. Sci. 2021, 7, 93−103